

Structure–Function Paradigm in Human Myoglobin: How a Single-Residue Substitution Affects NO Reactivity at Low pO₂

Mariano Andrea Scorciapino,^{†,‡} Enrico Spiga,^{†,⊗} Alessandra Vezzoli,^{||} Simona Mrakic-Spota,[⊥] Rosaria Russo,[⊥] Bruno Fink,[#] Mariano Casu,[†] Maristella Gussoni,^{*,⊥,∇} and Matteo Ceccarelli^{*,‡,†}

[†]Department of Chemical and Geological Sciences and [§]Department of Physical Sciences, University of Cagliari, Monserrato (CA), Italy

[‡]Istituto Officina dei Materiali del Consiglio Nazionale delle Ricerche (IOM-CNR), UOS, Cagliari, Italy

^{||}Institute for Bioimaging and Molecular Physiology, Consiglio Nazionale delle Ricerche (CNR), Segrate (MI), Italy

[⊥]Department of Pathophysiology and Transplantation–Physiology Section, University of Milan, Milan, Italy

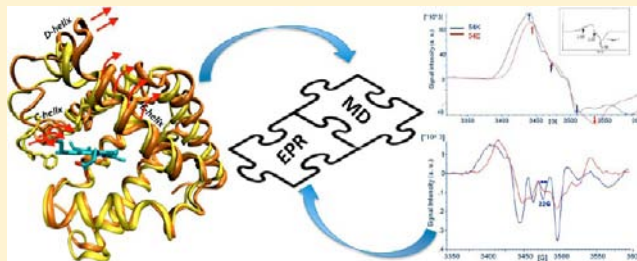
[#]Noxygen Science Transfer and Diagnostics GmbH, Elzach, Germany

[∇]Institute for Macromolecular Studies, CNR, Milan, Italy

Supporting Information

ABSTRACT: This work is focused on the two more expressed human myoglobin isoforms. In the literature, their different overexpression in high-altitude natives was proposed to be related to alternative/complementary functions in hypoxia. Interestingly, they differ only at residue-54, lysine or glutamate, which is external and far from the main binding site. In order to ascertain whether these two almost identical myoglobins might exert different functions and to contribute to a deeper understanding about myoglobin's oxygen-level dependent functioning, they have been compared with respect

to dynamics, heme electronic structure, and NO reactivity at different O₂ levels. Electron paramagnetic resonance (EPR) spectroscopy was employed to investigate the electronic structure of the nitrosyl-form, obtaining fundamental clues about a different bond interaction between the heme-iron and the proximal histidine and highlighting striking differences in NO reactivity, especially at a very low pO₂. The experimental results well matched with the information provided by molecular dynamics simulations, which showed a significantly different dynamics for the two proteins only in the absence of O₂. The single mutation differentiating the two myoglobins resulted in strongly affecting the plasticity of the CD-region (C-helix–loop–D-helix), whose fluctuations, being coupled to the solvent, were found to be correlated with the dynamics of the distal binding site. In the absence of O₂, on the one hand a significantly different probability for the histidine-gate opening has been shown by MD simulations, and on the other a different yield of myoglobin–NO formation was experimentally observed through EPR.



1. INTRODUCTION

For a very long time myoglobin (Mb) has been simply considered an O₂ storage/delivery system necessary to maintain its physiological concentration gradient across the cell, with prevalent expression in skeletal and cardiac muscle of mammals.^{1–5} However, more recent studies revealed its widespread expression in various nonmuscle tissues as well as in many other living organisms, including fishes, birds, reptiles, mollusks, and even bacteria and protozoa.⁶ In particular, an overexpression in response to hypoxia has been reported,^{7–9} with even possible implications in tumors' development.^{10,11} A relationship between Mb expression and hypoxia started to emerge, leading to the idea that this supposedly well-known protein might have alternative/complementary roles, such as NO scavenging¹² and NO₂[−] reduction,¹³ regulated by O₂ concentration.

NO is a highly diffusive and reactive molecule, produced, in the cells, by the NO synthases enzymes (NOS), using L-

arginine and O₂ as substrates.^{14,15} Among many different and fundamental roles as a signaling molecule, NO is a well-known inhibitor of the mitochondrial respiratory chain, having the cytochrome-*c*-oxidase as its primary target.¹⁶ Under normoxic conditions, if NO concentration becomes too high, oxy-Mb is able to scavenge and oxidize it to NO₃[−],^{17,18} maintaining mitochondrial O₂ consumption, thus cellular respiration, at the optimum. On the contrary, under hypoxia, the low O₂ availability leads to NOS inactivation (substrate limited). The few O₂ would be mostly consumed by the respiratory chain, resulting in a dramatic shortening of its concentration gradient through the tissue.^{16,19} However, in this condition, Mb was found to be able to act as a NO₂[−] reductase.^{13,17} The NO produced by Mb down-regulates mitochondria O₂ consumption, contributing to elongate the intracellular oxygen

Received: January 8, 2013

Published: April 30, 2013

gradient^{16,19} and limiting the formation of deleterious reactive oxygen species.²⁰ In addition, under hypoxia, Mb-produced NO might contribute to vasodilatation.²¹ The vasodilatory property of NO₂⁻, at physiological concentrations in vivo, has been previously described and associated to its conversion to NO by deoxy-hemoglobin.^{22,23} Then, the nitrite reductase activity of Mb at very low pO₂ levels, as it occurs during exercise or ischemia, has been associated to a rapid conversion of tissue nitrite to NO as well.^{16,19} Thus, Mb's nitrite reductase activity might participate both in the modulation of tissue mitochondrial respiration and in the limitation of ischemia-reperfusion injury, under hypoxic conditions.

In humans, up to five different Mb isoforms are reported in the literature, Mb-I (75–80%; pI 8.57), Mb-II (15–20%; pI 7.29), and Mb-III–V (all together 5%; pI 6.83).^{24,25} More recently, three alternatively spliced transcript variants, encoding for the same protein, have been reported.²⁶ Taking Mb-II as a reference, these proteins differ only by one external amino acid, and namely, they can be seen as the E54K (Mb I),²⁷ K133N (Mb III),²⁸ R139Q (Mb IV),²⁹ and R139W (Mb V)³⁰ mutants, whose specific functions, if any, are completely unknown.

In the context of the aforementioned O₂ level dependent multiple roles played by Mb, it is interesting to note that, when compared to low-landers, high altitude natives, like those from Tibet plateaus⁸ or Andean slopes,³¹ are characterized by a higher muscle Mb concentration. In particular, a recent proteomic investigation⁸ pointed out that the greater concentration of Mb in Tibetan natives (+20%) is totally attributable to the increase of the isoform Mb-II. Thus, together with the observation that Tibetans are also characterized by a higher efficiency of locomotion, a relationship between Mb-II overexpression and their evolutive adaptation to high altitude was put forward.^{8,32,33}

Now, focusing only on the two more expressed natural variants, the single-point mutation occurs in the CD-region (i.e., from residues 35 to 58, comprising the C- and the D-helices, together with the long loop in-between), whose motions upon photolysis, on the basis of time-resolved Laue crystallography experiments, have been suggested to be concerted with the piston-like movements of the E-helix, where the distal histidine (H64) is located, and to trigger, in addition, the swinging motions of the latter.^{34,35} This is particularly interesting, being H64's motions proposed to be mainly responsible for the opening and closing of the gate (the so-called histidine gate) between the protein external and the distal pocket (DP), which is the main ligand heme-binding site in Mb.^{36–43} Thus, if it was confirmed that CD-region's dynamics has a deep influence on the E-helix and H64's motions, it would be possible that specific mutations in that region might affect Mb's functioning. The CD-region's plasticity was also recently found to have a strong correlation with the transition from hexa- to penta-coordinate plants' hemoglobins.⁴⁴ Despite high sequence similarity, very few mutations seem able to alter protein structure and functions.⁴⁵

Human Mb has not been studied as extensively as those from other species. The only information available is the comparable O₂ and CO affinity of the human Mb isoforms.²⁴ After a very long gap in the literature, human Mb has been compared to those from horse and mouse, showing that the former is faster both as a NO scavenger in the presence of O₂ and as a nitrite reductase at a low O₂ level.¹⁷ In addition, the pO₂ might be particularly important, as highlighted in another very recent paper,⁴⁶ where many different mutants of sperm whale Mb have

been compared in terms of their O₂ storage and O₂ transport activity, separately. Important differences emerged only at a very low pO₂, and some organism-specific differences were also remarked, comparing the sperm whale to the human Mb.⁴⁶

However, no mention was made of the different isoforms, and in the light of all the above cited clues, the CD-region dynamics is certainly one of the aspects we are primarily interested in. In a recent experimental work of some of the authors,⁴⁷ the two more expressed human Mb isoforms have been structurally investigated through NMR spectroscopy. Both resulted in being stable in solution, and no heme loss has been observed, together with no significant structural differences in the heme region.⁴⁷ Possible allosteric effects on the internal cavities due to the single-point mutation were excluded,⁴⁷ thus addressing further investigations focused on the protein surface and the mutation region, by adopting other suitable techniques. In this regard, computer simulations represented one method of choice, since they provide an atomic-level description about proteins' thermal motions that may be difficult to obtain with experiments,⁴⁸ together with fundamental information on protein–solvent interplay.⁴⁹ In the present work, we compared the structure and dynamics of Mb-I and Mb-II, hereinafter referred to as S4K and S4E, respectively. The two more expressed human Mb isoforms were simulated in the three main forms, namely, deoxy-, oxy- and the aquomet-one, for more than 1 μ s each, without any energy bias and in the absence of ligands migrating inside the protein matrix, in order to capture the intrinsic protein motions created by spontaneous thermal fluctuations. Overall, the results of our simulations show how an external and single-point mutation plays an important influence on the dynamics of the DP, suggesting the possibility for a different affinity/reactivity toward one or more of the ligands that are key to Mb's functions.

On these bases, in order to take a first step toward the unveiling of possible different roles for these two human Mb isoforms, electron paramagnetic resonance (EPR) spectroscopy was also employed. EPR has been widely used for both structural and functional studies on different metalloproteins, to characterize, in particular, the symmetry of the electron density around radical species.^{50–52}

Under conditions as physiologic as possible, in the present study, a NO donor was incubated with the two more expressed human Mb isoforms in order to compare the amount of the Mb-NO complex formed at different pO₂ levels. From the present combined EPR/MD investigation, the two isoforms resulted in having an intriguingly different behavior tuned by the presence of oxygen, such that their differences became strikingly evident at a very low pO₂.

2. MATERIALS AND METHODS

2.1. Molecular Dynamics. Starting from the X-ray structure of a human Mb mutant (PDB code 3RGK at 2.8 Å) in the aquomet-form,⁵³ the R45K and A110C mutations led to the wild-type aquomet-S4E isoform. Then, the E54K mutation led to the aquomet-S4K isoform. Finally, the heme-bound water molecule was deleted or substituted with an oxygen molecule, to obtain the starting conformation for the corresponding deoxy- or oxy-forms, respectively. The two isoforms in the three forms were separately solved in an orthorhombic water box with an initial side length of 70 Å and containing 6680 water molecules (~22 500 atoms). Water molecules were placed far enough from the protein surface such that internal cavities were not occupied in the starting configuration. An initial slow heating from 10 to 300 K was carried out for 1 ns. Then, 50 ns were simulated in the NPT ensemble at 1.0 bar and 300 K allowing for

waters rearrangement and box equilibration. Finally, 1.1–1.5 μs MD simulations were performed in the NVT ensemble with a Langevin thermostat and using the average box dimensions from the previous simulation, saving the coordinates every 50 ps. All MD simulations were performed employing the Amber99SB-ILDN force field⁵⁴ and TIP3P⁵⁵ for the protein (and heme group) and waters, respectively. The soft particle mesh Ewald (SPME) algorithm (64 grid points and order 4 with direct cutoff at 1.0 nm) was used to treat long-range electrostatic contributions, within the ACEMD package⁵⁶ compiled for GPUs. Hydrogen bonds and secondary structure analysis were carried out with the Simulaid package.⁵⁷ Cavities calculations were performed with an iterative application of the software VOIDOO.^{58,59}

Water/protein interactions time scales were quantitatively investigated computing the so-called survival probability function for the bonds between solvent molecules and the protein:⁶⁰

$$N_w(t) = \frac{1}{N_t} \sum_{n=1}^{N_t} \sum_j P_j(t_n, t) \quad (1)$$

where, t is the time, N_t is the total number of water molecules, and $P_j(t_n, t)$ is a function that takes the values of 1 if the j^{th} water molecule is found within a certain cutoff from the protein, between time t and $t + t_n$, zero otherwise. A different cut off R_{cut} is computed for any couples of water and protein atoms, such that $R_{\text{cut}} = f(r_w + r_p)$, where r_w and r_p are the van der Waals radii obtained from the force field for water and protein atoms, respectively, while f is a pre factor equal to 1.1.⁶¹ In this kind of calculation, due to the relatively short correlation time of the water molecules, system coordinates need to be saved quite often (500 fs), in order to sample even the shortest residence time waters. Thus, additional ad-hoc simulations were performed on the oxy forms, with a total simulation time of ~ 100 ns. This time was set on the basis of the corresponding survival probability of the water molecules, which converged to 0 within the simulated time, due to the lack of permanently bound waters. This indicates, in turn, that all the water molecules were in exchange with the bulk solvent in that range.

Interested readers can find additional details about simulations setup and the algorithms used, in the Supporting Information (SI). Technical information about the software 'Simulaid' used for secondary structure and hydrogen bonds (H-bonds) analysis as well as about the software 'Modeler' used to prepare the starting structures are also provided.

2.2. Electron Paramagnetic Resonance. 2.2.1. Protein Samples Preparation. Both 54K and 54E human Mbs were purchased from Asla (Riga, Latvia) and provided in the aquomet form. They have been obtained by site-directed mutagenesis PCR approach and expressed in *Escherichia coli* BL21(DE3) cells (Novagen).

2.2.2. EPR Samples. The EPR experiments were carried out on the two proteins in the nitrosyl-Mb form, dissolved in degassed Krebs-Hepes buffer (20 mM, Noxygen Elzach). The pH was adjusted to 7.4 by the addition of small aliquots of NaOH (0.1M). First, in order to compare our spectra to those reported in the literature, the starting ferric proteins were reduced by the addition of freshly prepared 100 mM sodium dithionite (SDT, Sigma) under free-O₂ condition. The ferrous deoxy-proteins were then incubated in a temperature and gas treatment chamber (BIOV, Noxygen) in the presence of the NO donor (0.05 mM, MAHMA-NONOate, Alexis Biochemicals corporation) for 30 min at 310 K. Thus, the incubation started with the deoxy being the only Mb form present in solution. Moreover, in the absence of oxygen, free-NO and/or NO-Mb side reactions with O₂ have been prevented.

Second, in order to investigate the Mb-NO complex formation in a condition as physiological as possible, the addition of reducing reagents was avoided: the two proteins, in the aquomet-form, were incubated at three different O₂ concentrations, i.e., pO₂ = 0, 40, and 200 mmHg. The solutions were incubated as before: 30 min at 310 K in a temperature and gas treatment chamber, in the presence of the NO donor at the chosen pO₂ level. After incubation, each sample (400 μL) was put under liquid nitrogen overnight.

2.2.3. pO₂ Calibration. EPR experiments, as said, were carried out at three different values of pO₂ = 0, 40, 200 mmHg. While the lowest

and highest level were easily obtained by incubating the Mb samples (in the presence of the NO donor) in the treatment chamber under 100% N₂ or 21% O₂ gas flow, respectively, a pO₂ calibration had to be performed, in order to establish the incubation time necessary to reach the pO₂ = 40 mmHg. To this aim, the oxyethidium (3,8-diamino-5-oxy-6-hydro-5-ethyl-6-phenylphenanthridine, Noxygen) radical (4 μM) was dissolved in buffer and put in apposite O₂ permeable capillaries (40 μL final volume). N₂ (100%) was previously flowed into the capillaries to completely remove O₂ from the solution. At regular time intervals, one of the aliquots was taken out of the chamber and put in a glass capillary for EPR analysis at 310 K.

The intensity of the samples' EPR signal decreased with decreasing pO₂, starting from the maximum obtained at pO₂ = 200 mmHg, until only a low-intensity residual resonance due to the oxyethidium radical's signal alone (incubation time 0 min; pO₂ = 0) was observed. From the built-up calibration curve (signal amplitude versus incubation time, not shown), the degassed samples were thus incubated for 30 min at 310K to attain a pO₂ level of 40 mmHg.

2.2.4. EPR Measurements. EPR experiments were carried out on frozen samples in a EPR tube, held by a finger-tip liquid nitrogen dewar. An E-SCAN spectrometer (Bruker) was used, operating at the X band. All the spectra were recorded at 77 K, adopting the same acquisition parameters: 10 scans on average, 5.24 s sweep time, 8.16 G modulation amplitude, 86 kHz modulation frequency, 42 mW microwave power at a frequency of 9.786 GHz. EPR spectra were baseline corrected, and the normalized spectral area (au) calculated by double integration, using the standard EPR software supplied by Bruker (WinEPR, version 3.1). Four repetitions were performed for each experiment.

In order to convert the EPR signals areas (au) into concentrations (μM), a calibration was performed following the procedure reported in the literature.^{62,63} Proteins were reduced by the addition of freshly prepared sodium dithionite under free-O₂ condition, and the presence of a unique form was checked by UV-vis spectrometry. Proteins were then incubated with known amount of the NO donor (10–50 μM range), and a linear signal area/concentration relationship was found as expected. These calibration curves are provided in the SI.

As already pointed out, since EPR experiments were also carried out after the incubation with the NO-donor, starting from the two proteins in the aquomet-form, a preliminary investigation was carried out, in order to ascertain that the EPR spectrum of the latter did not interfere with that of the nitrosyl-form we were interested in.

2.2.5. Statistical Analysis. Statistical analysis was performed using the GraphPad Prism package (GraphPad Prism 5, Software Inc. San Diego, CA). Data were analyzed using repeated Shapiro-Wilk W tests. In the Shapiro-Wilk W test, the null hypothesis is that the sample is taken from a normal distribution. This hypothesis is rejected if the critical value P for the statistic test W is < 0.05 . Experimental data collected at the different pO₂ values were compared using one-way ANOVA with a Tukey posthoc test. $P < 0.05$ statistical significance level was accepted. The results were reported as mean values \pm standard deviation (SD).

3. RESULTS AND DISCUSSION

3.1. Molecular Dynamics. 3.1.1. Conformational Flexibility of the CD Region. Fluctuations were calculated on the basis of C α 's positions. Figure S1 shows the results obtained for the CD-region of both the isoforms, either in the deoxy-, oxy-, and the aquomet-form. This flexible region resulted in having slightly higher fluctuations in the 54K than in the 54E isoform, in all of the investigated cases. However, it is interesting to note how fluctuations were generally reduced in the oxy-form (Figure S1b) for both the human Mbs, until the difference among the two became negligible. The highest values were always observed around the 43th residue, a phenylalanine, which is located at the very beginning of the long loop separating the C- from the D-helix.

Table 1. Intramolecular H-Bonds Formed by the 54th Residue of the 54K and 54E Human Mb Isoforms, Either in the Deoxy-, Aquomet-, and Oxy-form

deoxy-54K			aquomet-54K			oxy-54K		
donor	acceptor	occurrence ^a [%]	donor	acceptor	occurrence ^a [%]	donor	acceptor	occurrence ^a [%]
S58-H γ	K54-O	24.3	S58-H γ	K54-O	24.2	S58-H γ	K54-O	47.1
K54-H ζ	D53-O δ	11.0	K54-H ζ	D53-O δ	13.1	K54-H ζ	D53-O δ	11.3
deoxy-54E			aquomet-54E			oxy-54E		
donor	acceptor	occurrence ^a [%]	donor	acceptor	occurrence ^a [%]	donor	acceptor	occurrence ^a [%]
K50-H N	E54-O ϵ	43.4	K50-H N	E54-O ϵ	43.2	S58-H γ	E54-O	46.6
S58-H γ	E54-O	43.1	S58-H γ	E54-O	37.7	K50-H N	E54-O ϵ	38.6
K50-H ζ	E54-O ϵ	14.4	K50-H ζ	E54-O ϵ	12.3	K50-H ζ	E54-O ϵ	12.3

^aOnly the H-bonds with an occurrence >10% are reported.

These differences in the fluctuations were reflected by those found in the secondary structure. The relative probability of the different motives (only the α -helix, 3_{10} helix, and unordered structure were observed) has been calculated for each of the residues in the CD-region, on the basis of the secondary structure adopted in each of the frames along our MD trajectories. Figure S2 shows the results obtained for the unordered structure and the α -helix. The 54K isoform resulted in having a higher conformational plasticity than the 54E. The CD-region's backbone of the former, indeed, was found to change secondary structure more often. Again, it is interesting to note how the two Mb isoforms were comparable in the oxy-form.

Correspondingly, in the case of 54E isoform, the carboxyl-group of the glutamate's side-chain was found to be a very good H-bond acceptor, while the amino-group of the lysine's side-chain in the 54K, resulted in being only a poor H-bond donor. In Table 1 the H-bonds formed (with an occurrence >10%) by the 54th residue of both isoforms are reported. In all the cases, the 54E's glutamate formed more stable H-bonds, comprising, in particular, the backbone amide group of the residue 50, which is located in the loop separating the C- and the D-helix. On the other hand, the 54K's lysine formed less stable H-bonds, mainly involving the side-chain of its nearest neighbors.

Thus, summarizing, the occurrence and the number of the H-bonds formed by the mutated residue, with other residues located in the CD-region, seem to be inversely correlated with the CD-region's conformational plasticity. Either in the deoxy- or the aquomet-form, 54E was found to have a more rigid CD-region than the 54K isoform. However, in the oxy-form, despite the differences in the H-bonds of the CD-region remained almost the same, the two human Mbs were much more comparable with each other in terms of CD-region plasticity, both experiencing a structural tightening, probably due to the relatively strong coordination of the bound O₂ by the residue H64.

As already mentioned in the introduction, despite the single-point mutation differentiating the two human Mbs, it was particularly interesting to find some differences in the dynamics of the whole CD-region. This is surely one of the most flexible portions of Mb, due to the presence of a \sim 10-mer loop, but its dynamics was already found to be coupled to that of the E-helix in previous time-resolved Laue crystallography investigations.^{34,35} This technique, which actually probes the relaxation, following a photolysis event, from a nonequilibrium deoxy-state back to the ligated state, provided an indication of a possible coupling between the dynamics of the CD-region and the DP. On the other hand, MD simulations, that sample spontaneous

thermal fluctuations, showed that this coupling is 'active' even at the equilibrium, characterizing the intrinsic dynamic behavior of the protein (see Section 3.1.2).

However, it has to be stressed that a single specific mutation per se, should not be automatically related to an altered dynamics. The same mutation, in a Mb other than the human one, might be ineffective at all, since, of course, the overall dynamics is determined by the specific entire amino acid sequence of the protein's portion investigated. Indeed, organism-specific differences in Mb's reactivity were put forward in recent experimental investigations,^{17,46} and the oxygen level was shown to be fundamental in highlighting possible differences among mutants.⁴⁶ In our case, it was interesting to find that while comparing the deoxy-forms, these differences were somewhat emphasized on one hand, and they were somehow repressed in the case of the oxy-forms, on the other. By the way, this strongly supports the hypothesis that the two human Mb isoforms might have a different behavior only at a low pO₂.

In the literature, it was suggested that CD-region mobility might be solvent slaved.^{34,35} Actually, a variety of proteins display solvent slaved processes, including Mb.^{49,64–66} Solvent motions dominate a broad range of processes, from conformational fluctuations and relaxations, to ligand migration and catalysis. Solvent dynamics around protein is primarily affected by surface local shape and the specific amino acids composition, being external side chains groups fundamental as H-donors or H-acceptors with respect to hydration waters, ultimately affecting their dynamics and, thus, the stability of the hydration shell.⁶⁷ In particular, recently, "a unified model of proteins dynamics" has been formulated on the basis of an extended experimental work.⁶⁸ Large-scale protein motions were shown to be slaved to the fluctuations in the bulk solvent and controlled by the solvent viscosity on one hand, while internal motions to be slaved to the fluctuations of the hydration shell, on the other. Thus, investigation of protein/solvent interactions is crucial to fully capture the dynamics of the system as a whole.

In order to investigate the influence of the mutated residue on the dynamics of the CD-region, protein/solvent interactions were studied too. In particular, as described in the Methods section, the survival probability function was computed for the waters comprised in the hydration shell of the CD-region (Figure S3). The observed differences in CD-region's plasticity, accompanied by those found in H-bonding propensity of the mutated residue, were further reflected by a different waters' survival probability function. In the case of 54K, the faster dynamics of the CD-region's hydration shell is shown by a steeper decreasing curve, in agreement with a higher conforma-

tional plasticity. On average, 54E had one long residence-time water (from 50 ps to 1 ns) more than 54K, indeed, though the lysine has a longer side chain than glutamate. These results are in agreement with a recent investigation about water dynamics around the different amino acids, where the critical role played by hydrophilic proton acceptors on water dynamics has been highlighted, in accord with various experimental observations.⁶⁷ Donor groups, like the lysine N_2H_3 , resulted in having an effect analogous to the hydrophobic groups, slightly retarding water dynamics (with respect to the self-diffusion in the bulk). On the contrary, strong H-acceptors, such as the carboxylic group of the aspartic and glutamic acid, were shown to be able to induce a pronounced slowdown of water hydration dynamics.

3.1.2. Volume Fluctuations of the Distal Pocket. As described in detail elsewhere,⁴⁸ internal cavities' volume calculation can be iteratively applied to a MD trajectory, resulting in a statistical characterization of their fluctuations, in terms of distinct volume states.

Figure 1a shows DP's volume probability distribution obtained for both the 54K and 54E isoforms in the deoxy-form. It was clearly bimodal, with mean values equal to 14.8 and 35.9 Å³ in the former 16.0 and 46.3 Å³ in the latter. In the 54E isoform, the DP showed a significantly higher probability to expand than observed for the 54K. The in-depth analysis of the residues actually lining the cavity in the two different volume states showed that this expansion mostly occurred toward either the C-helix or the first part of the long loop separating the latter from the D one. It was really interesting to find that DP expansion was directed toward the portion where the aforementioned F43 residue is located, which was characterized by the largest fluctuations among the CD-region.

Figure 1b shows the representative structure for the so-called compact state of the DP, while Figure 1c shows that for the expanded state, together with the residues lining the cavity. A closer inspection of the structural differences between these two states indicated the involvement of the CD-region in the DP volume fluctuations, indeed.

Figure 2 shows the comparison of the two structures zoomed in Figure 1b,c. The expansion of the DP resulted in being mainly due to a slight shift of the first part of the E-helix, leading to the distal histidine moving slightly far from the iron. Moreover, this movement was found to be accompanied by the shift of the D-helix as well, together with both the C-helix and the CD-loop moving upwards and backwards in the figure. These structural changes, already observed by a previous experimental investigation,³⁴ resulted in the C-helix moving closer to the heme, leaving more space for DP accessibility from the external.

Figure S4 shows the DP's volume as a function of simulation time together with the distance of both the residue H64 (i.e., the distal histidine) and the F43 from the iron. A general correlation was found between these two distances and the DP's volume. As expected, a positive correlation was found with the former and a negative one with the latter. These correlations were found for both the Mb isoforms, but not surprisingly, they resulted in being more evident in the 54E, considering the fact that in the 54K, DP's volume fluctuations were not as marked. These observations indicated, in turn, that the two aforementioned distances were anticorrelated. Indeed, a more comprehensive picture could be obtained by computing the corresponding cross-correlation distributions (Figure 3). While the 54K was found mostly in the compact state, the 54E clearly passed from the compact to the expanded state, showing

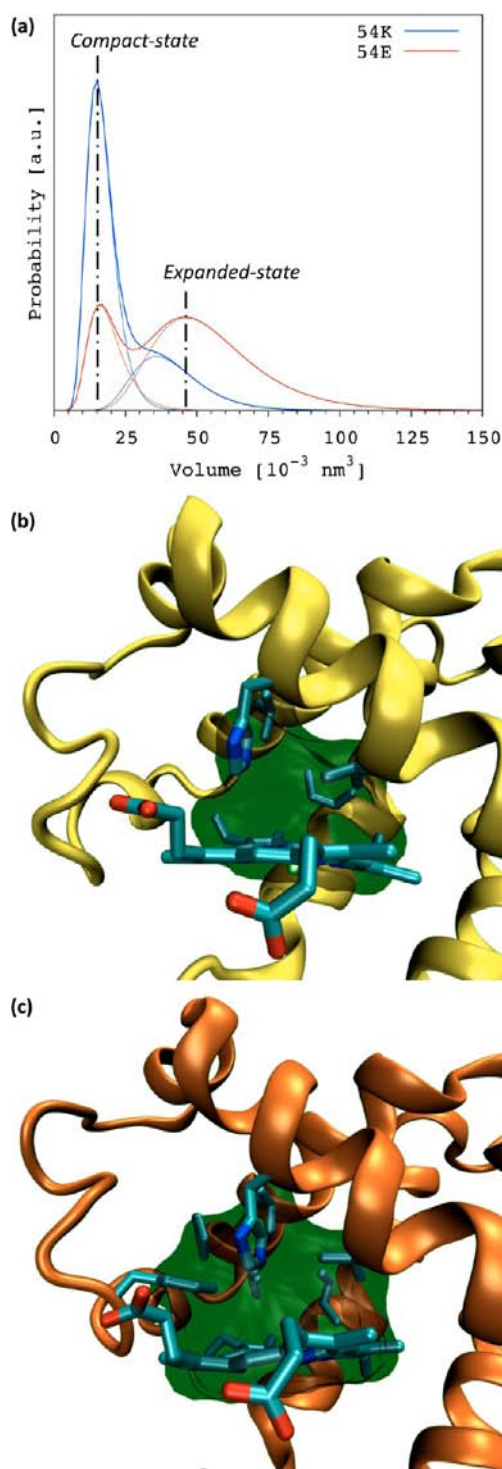


Figure 1. DP's volume distribution is shown in (a) for the deoxy-54K and deoxy-54E isoforms. The representative structure of the (b) compact-state and (c) expanded-state of the DP is shown, together with the residues actually lining the cavity. The volume of the latter is represented with the shadowed area.

a striking difference between the dynamics of the two human Mbs, when compared in the deoxy-form.

On the other hand, in accord with what has been shown for CD-region's fluctuations and secondary structure, the two Mb isoforms resulted in being almost comparable, when compared in the oxy-form. Figure 4-a shows the DP's volume distributions. The latter were, again, bimodal with mean values

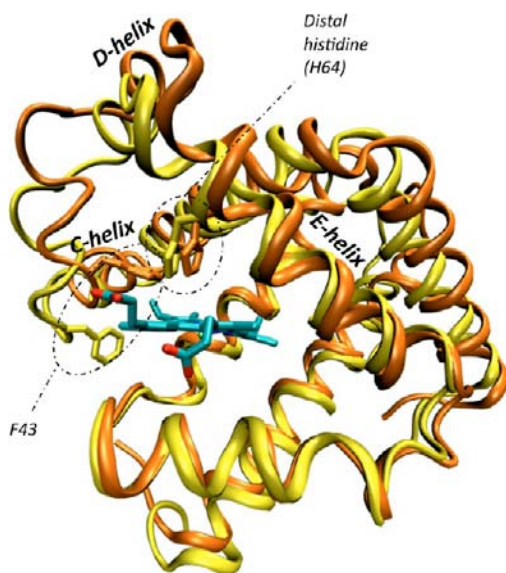


Figure 2. Representative structure for the compact (yellow) and expanded (orange) states of the DP in the deoxy-form has been superimposed to be compared, revealing the structural changes accompanying DP's volume fluctuations.

equal to 15.8 and 45.3 Å³ for the 54K, 15.1 and 41.3 Å³ for the 54E. Differently from the case of the deoxy-forms, the DP expansion occurred toward the neighboring Xe4 cavity, thus, toward the protein interior, with a comparable probability. Figure 4-b and 4-c show the representative structure for the two distinct volume states.

Again, a general positive correlation was found between the DP's volume and the distance between the H64–C α and the iron as well as a general negative correlation with the distance of F43–C α and the iron (Figure S5). However, in the case of the oxy-forms, since DP's expansion occurred toward the Xe4 cavity, as said, the contribution of the residues comprising the DP/Xe4 gate resulted in being much more important on the DP's volume fluctuations, than observed for the deoxy-forms. Nevertheless, the anticorrelation between the distance of H64 and F43 from the iron was still evident, with the cross-

correlation distributions further showing the similarity between the dynamics of the two oxy-isoforms in the protein region under investigation (Figure 5).

The aquomet-forms resulted in having a dynamical behavior slightly different from that of either the corresponding deoxy- and the oxy-forms. Nevertheless, the major general differences found between the two deoxy-Mb isoforms resulted in being confirmed. Figure S6a shows the DP's volume distribution. Its dynamics was clearly different comparing the two Mb isoforms and similar to what was observed in the case of the deoxy-forms, while the 54K had the highest probability for relatively small volumes, the 54E showed a higher probability for DP expansion toward the exterior. Figure S6b shows the probability distribution of the distance between H64–C α and the heme-iron. Indeed, the 54E was characterized by a higher probability for longer distances than the 54K.

These observations were reflected, in turn, by a dramatic difference in the probability for the “classic” histidine-gate opening.^{36–43} Indeed, the δ protonation state of the H64 “activated” the latter in both the isoforms. Figure 6 shows the probability distribution computed for the torsion of the H64's side chain around the C α –C β bond. Two distinct states were found for both the isoforms, one corresponding to the open and the other to the close state of the histidine gate. However, their relative probability was dramatically different for the two human Mb isoform, with the 54E being found for 63% of the time in the open conformation while only 54K, vice versa, for the 27%. For example, the movie S1 shows the trajectory of the aquomet-54E, where the aforementioned twisting motions of H64's side-chain can be observed.

Summarizing, the above-mentioned differences found in the CD-region's dynamics were reflected by significant differences in that of the DP, confirming that the motions of these two Mb's regions are concerted.^{34,35} Thermal fluctuations of the hydration shell are transferred to the protein surface, and then, the fluctuations induced in the latter affect those of the protein interior.⁶⁸ It is possible to speculate that the energy transferred from the solvent to the CD-region is “dissipated” in the 54K isoform as conformational changes, having a little effect on the dynamics of the adjacent distal region. On the other hand, 54E has a more rigid CD-region where conformational changes are

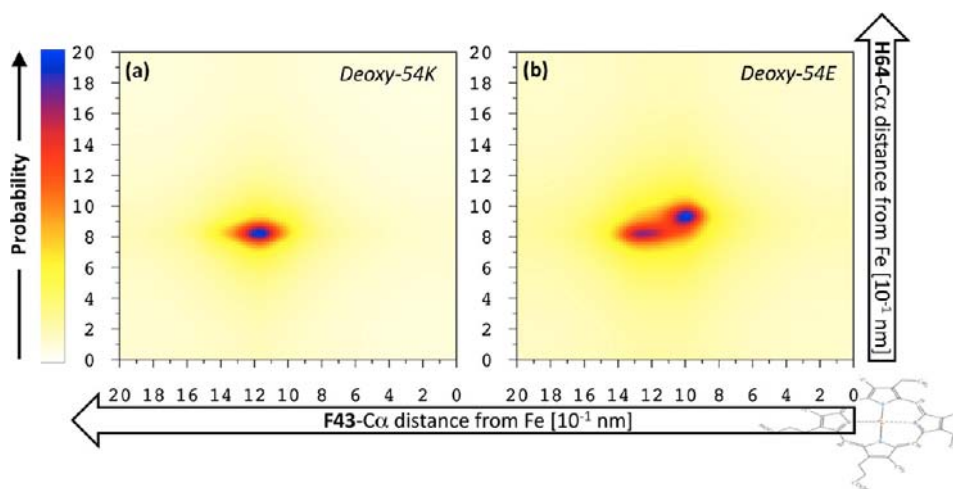


Figure 3. Cross-correlation distribution for the distance of H64–C α from the heme-iron and F43–C α from the heme-iron is shown as a two-dimensional map, for the deoxy-state of both Mb isoforms. Probability, which is plotted on the z-axis, has been color-coded as shown by the box on the left. Note that x-axis direction has been inverted in order to reflect the same perspective of Figures 1 and 2.

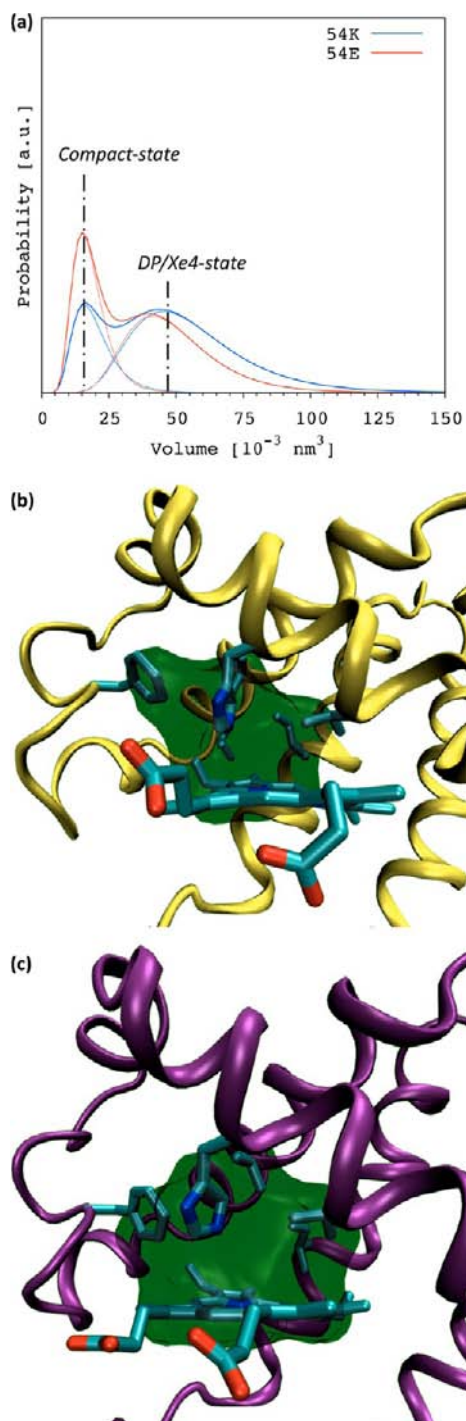


Figure 4. DP's volume distribution is shown in (a) for the oxy-54K and oxy-54E isoforms. The representative structure of the (b) compact and (c) DP/Xe4 states of the DP is shown, together with the residues actually lining the cavity. The volume of the latter is represented with the shadowed area.

somewhat hindered. Thus, the energy coming from the solvent is translated into quasi-rigid motions that can be transferred to the E-helix via the D one. However, when a ligand like the oxygen binds the iron and is strongly coordinated by the distal histidine, the DP experiences a structural tightening, which opposes to the coupling with CD-region fluctuations.

This, of course, is merely a speculation, but in light of our results, we could hypothesize a possible different binding

efficacy for the two human Mbs in the absence of oxygen, since our MDs showed that both the deoxy- and the aquomet-forms have a remarkably different behavior. In particular, 54E was expected to be more prone to ligand binding than 54K, being found to open more often toward the external and thus being more probable for a ligand to come into the heme pocket. In the literature, a comparable affinity is shown for O_2 ,²⁴ but no one investigation is reported about functioning at low pO_2 . Our hypothesis was supported and complemented by the EPR investigations reported hereinafter, further sustaining the leading idea that a different reactivity of the two human Mbs could be possibly emphasized under severe hypoxic conditions.

Finally, for the sake of completeness, it should be noted that, in principle, all of the differences found between the two Mbs can be considered statistically significant only if they result in being larger than the difference observed in different MD simulations replicas performed on the same protein, in the same form, and starting from different initial conformations. As reported in the SI in more details, in the present work the authors preferred to perform long simulations, in order to check system stability on a long time-range. However, in order to introduce additional noise and achieve a better sampling of the conformational space, we stopped and restarted simulations every 200 ns, generating new velocities with a different seed for random numbers. A statistical analysis was performed by treating each of the 200 ns windows as an independent simulation, namely the block average method. The standard deviation of the calculated probabilities (e.g., DP compact/expanded and H64 open/close conformation) resulted in being 15% at most, which is less than the difference observed comparing the two isoforms.

3.2. EPR. Figure 7a shows the spectra of both the 54K and 54E human Mb isoforms (0.05 mM), recorded after reduction to the deoxy-form and subsequent incubation in the presence of the NO donor, in the absence of oxygen. For example, the displayed spectra are relative to the 0.05 mM donor concentration and have not been normalized to allow a better comparison. Both the spectra closely resemble that previously reported in the literature,⁶⁹ which is shown in the inset, and that the spectrum was obtained from the “native” human Mb in the nitrosyl form under anaerobic conditions, i.e., the same conditions we employed.

The peculiar spectral shape, similar in both the proteins, suggested the formation of the nitrosyl-Mb form. In fact, as can be observed in the figure, although the peaks are somewhat broad and partially overlapped, both absorption curves show the characteristics of a system endowed with a rhombic symmetry around the paramagnetic center.⁵¹ Three effective g values could be detected in the spectra: one peak on each side of the horizontal line was identified as the x and y in-plane absorption (g_x and g_y), whose directions are mutually perpendicular and approximately parallel to the heme plane. Their g values were 2.0270 ± 0.0002 (g_x) and 1.9866 ± 0.0001 (g_y), 2.0258 ± 0.0004 (g_x) and 1.9730 ± 0.0037 (g_y) for the 54K and 54E isoforms, respectively. In between, an ‘inverted S shape’ is displayed, located at $g \approx 2.00$ for both the proteins. The axial absorption, i.e., the g_z factor, showed the hyperfine splitting due to the NO nitrogen and was found at 2.0072 ± 0.0004 and 1.9985 ± 0.0050 for 54K and 54E, respectively. From the EPR spectrum of the “native” human nitrosyl-Mb, g factors approximately equal to 2.08 (g_x), 2.01 (g_z), and 1.98 (g_y) have been previously reported in the literature⁶⁹ (see the inset in Figure 7b).

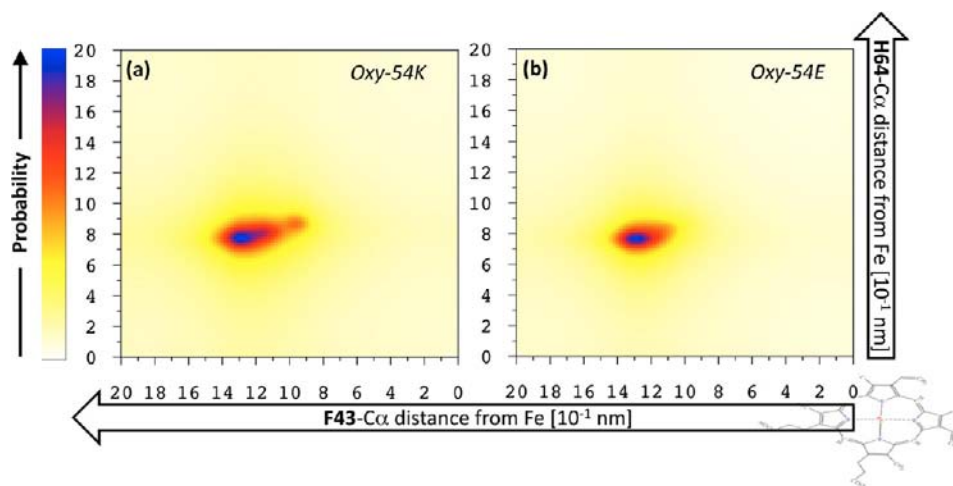


Figure 5. Cross-correlation distribution for the distance of H64–C α from the heme-iron and F43–C α from the heme-iron is shown as a two-dimensional map, for the oxy-state of both Mb isoforms. Probability, which is plotted on the z-axis, has been color-coded as shown by the box on the left. Note that x-axis direction has been inverted in order to reflect the same perspective of Figure 4.

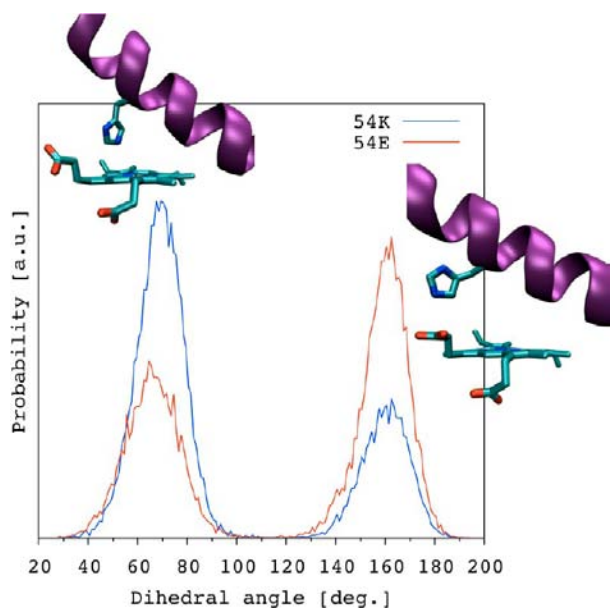


Figure 6. Probability distribution of the H64's side chain torsion around the C α –C β bond for both the 54K and 54E isoform in the aquomet-state. The position of the distal histidine in the two distinct states is shown in the two corresponding insets.

As expected, the g factors of the two proteins were found to significantly deviate from the free electron spin value (2.0023),⁵¹ indicating that the 3d orbitals of the iron ion are strongly involved, as a result of the spin–orbit interaction. Indeed, this deviation is generally found to be inversely proportional to the energy separation between the orbital of the unpaired electron and those coupled to it by a spin–orbit interaction,⁷⁰ such that, stronger is the electric field surrounding the unpaired electron and larger this orbitals' energy separation. Thus, an increase in the g factors indicates a lowering of the energy for the unpaired electron's orbital with respect to the others. The unpaired electron is not strongly localized on the iron-bound NO but is partially delocalized over the Fe 3d orbitals.⁵¹

A slightly different in-plane anisotropy was found upon comparison of the two Mbs' spectra (as resulted by the g_x and

g_y resonances peak-to-peak separation), with the 54E being shifted upfield with respect to 54K. In particular, the degree of the p_π – d_π interactions between the orbitals of either the proximal ligand and/or the nitric oxide with the heme were considered to determine the in-plane anisotropy.⁷¹

At the same time, a superhyperfine interaction with another axially bound ^{14}N nucleus should be expected: the sixth ligand of the heme-iron was identified as the unprotonated nitrogen belonging to the residue H93 (i.e., the proximal histidine) and the coupling constant of the hyperfine splitting of resonance lines, due to the covalent bond between heme-iron and this residue, estimated to be $\sim 22\text{G}$ (Figure 7b).⁵⁰ Indeed, in a hexacoordinate nitrosyl-form, a nine-line hyperfine splitting is theoretically expected, originating from the interaction of the unpaired electron both with the ^{14}NO nitrogen and the ^{14}N nucleus of the axial base located in *trans* to the NO. The exact number of components or factors contributing to a given spectrum has been previously established, and three species of nitrosyl-ferro-heme complexes identified, strictly depending on the strength of the interaction between the iron and the axial base nitrogen. This, in turn, resulted in being related to the bond distance between the iron and the base nitrogen,⁷² up to the rupture of the iron–N ϵ bond associated to the addition of a proton to the metal-bound imidazole in the pentacoordinate form.⁷³

From the spectra (Figure 7), it is evident that the two proteins showed a different superhyperfine interaction, with the 54E showing an almost axial symmetry. This difference could be also observed when spectra were recorded under $p\text{O}_2 = 40$ mmHg starting from the aquomet-form (Figure S7). These results suggest a different unpaired electron interaction with the axial base nitrogen for the two proteins, which is attributable to a stronger bond between the H93 and the iron for 54E than 54K.

As described in the Section 2, the formation of the Mb-NO complex was monitored for the two human isoforms at three different $p\text{O}_2$ values (0, 40, and 200 mmHg), starting from the proteins in the aquomet-form. This experimental setup was chosen in order to compare the two proteins in a condition as physiological as possible. To this aim, first of all, the addition of a large excess of a strong reducing agent, such as sodium dithionite, which surely does not resemble a physiological

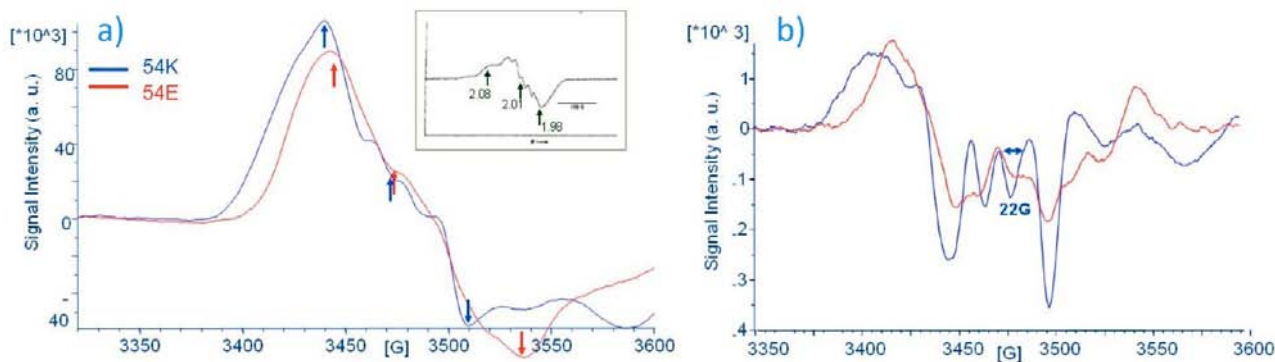


Figure 7. (a) EPR spectrum of the nitrosyl-form is shown for both the isoforms. Spectra were not normalized to allow for a better comparison. Three distinct g values are shown, indicated by the arrows; 54K: $g_x = 2.03$, $g_z = 2.00$, $g_y = 1.99$; and 54E: $g_x = 2.02$, $g_z = 1.99$, $g_y = 1.97$. An EPR spectrum reported in the literature for the “native” human nitrosyl-Mb is shown in the inset, and the g factors indicated. (b) The second derivative of the spectra reported in (a) is shown. The difference between the spectra is emphasized, and in particular, the z -hyperfine coupling constant of 22G is marked.

environment, was intentionally avoided. The pO_2 levels were in turn chosen to mirror three well-known physiological conditions: the extreme hypoxia ($pO_2 = 0$), the resting O_2 partial pressure in venous blood and interstitial space of peripheral tissues ($pO_2 = 40$ mmHg), and the “maximum” O_2 concentration reached on air-exposure, respectively. Moreover, it is important to stress here that $pO_2 = 40$ mmHg was also found to correspond to the maximum efficiency of the NO donor employed, when both NO generation and its oxidation to NO_2^- in the presence of O_2 are taken into account.⁷⁴ On the other hand, on air exposure, NO oxidation reaches the maximum and, in turn, NO availability the minimum. This was probably one of the reasons why, in a previous study,⁶⁹ the EPR signal could not be detected when starting from the aquomet-form for either horse and human Mbs. The same authors stated that their results were in contrast with other studies about Mb-NO formation that were performed, indeed, at low pO_2 .^{75,76}

Particular attention was paid to establish the NO donor concentration to be adopted. The necessity of avoiding the use of a large excess of NO (e.g., 10-fold greater) has been previously pointed out as one of the main aspects to be taken into account to model, *in vitro*, a physiological environment. In fact, the ‘*in vivo*’ NO/hemoglobin concentration ratio is strikingly different, being the NO concentration ~ 1000 fold lower than Hb.⁷⁷ The specific NO donor concentration adopted in the present work was therefore considered to be a good compromise between the actual physiological value and, considering the yield of the reaction, the needing for a final concentration of the nitrosyl-Mb over the detection limit of our EPR spectrometer.

The final concentration of Mb-NO formed is reported in Figure 8 for both human isoforms, as a function of the oxygen concentration. A significantly larger concentration was determined for 54E under deoxygenated conditions, while comparable results were obtained in the presence of oxygen. These results clearly support a different behavior of the two more expressed human Mb isoforms at a very low pO_2 . However, Mb reductive nitrosylation is a multistep process involving NO binding to $(Fe^{3+})Mb$, subsequent iron reduction through a reaction with OH^- (and release of nitrous acid) and binding of a second NO to $(Fe^{2+})Mb$.⁷⁸ Thus, from the present data it cannot be concluded whether this observed difference is

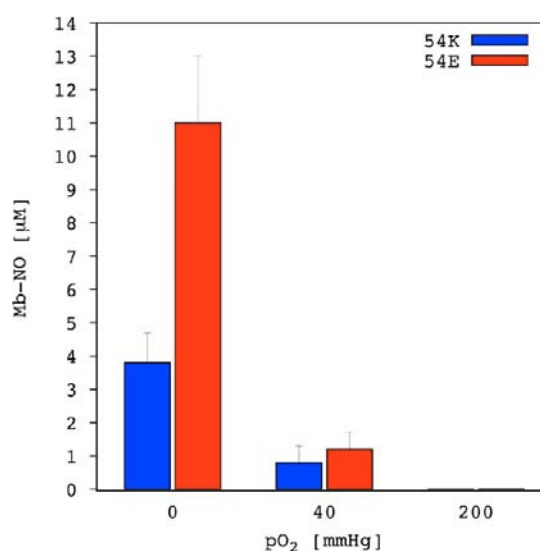


Figure 8. Histogram of Mb-NO formed starting from either 54K or 54E in the aquomet-form (0.05 mM), after incubation with the NO donor (0.05 mM) at different pO_2 levels. Standard deviation (error bars) was calculated from four independent measurements.

due to an altered NO binding equilibrium and/or different rate of some of the nitrosylation process steps.

In the presence of oxygen, the situation is even more complicated, since a number of other reactions can take place, lowering the concentration of Mb-NO. For instance, the NO produced by the donor could be oxidized to NO_2^- , reducing NO availability and possibly forming the Mb- NO_2^- complex. In addition, the oxygen molecule is able to react with the iron-bound NO to form the aquomet-Mb and NO_3^- . In other words, the almost equal Mb-NO concentration we measured in the presence of oxygen cannot be straightforwardly interpreted in terms of an equal behavior of the two human Mbs, since differences in one or more of the possible reactions could compensate each other and lead to a comparable amount of Mb-NO as well. Thus, while in the absence of O_2 , a different behavior is evident from the present work, whether the two human Mb isoforms might preserve some differences with increasing the pO_2 remains an open point.

4. CONCLUSIONS

The relevance of the hypoxic conditions that are encountered both in physiological and pathological situations, in conjunction with the multiple roles attributed to Mb, were the rational basis for the present study. In addition to these general observations, our interest arose from the specific findings on populations born and living in extreme hypoxic conditions, whose higher Mb concentration might possibly explain the reported better metabolic and mechanic efficiency, with particular reference to the 54E isoform.

Throughout a combined EPR and MD investigation, the two more expressed human Mb isoforms, namely 54K and 54E, have been compared in the present study. In order to contribute to the understanding of the relevant roles played by Mb under hypoxic conditions, a first step was taken toward the identification of the dynamical and functional differences between these two human Mbs.

In particular, the following hypothesis could be put forward: A quite rigid CD-region results in a strong coupling between the solvent thermal fluctuations and the piston-like movements of the heme distal region, on one hand, and a CD-region characterized by a higher plasticity allows to 'dissipate' the thermal energy coming from the solvent by conformational changes, leading to a weakened coupling between the dynamics of the CD-region and the DP, on the other. Ultimately, enhanced fluctuations of the DP, resulting in a higher probability for the histidine gate opening, are expected to be mirrored by an easier ligand entrance and, possibly, an higher probability for its binding to the iron.

The present investigation has shown that the dynamics of the CD-region and that of the DP are strongly correlated. In turn, the latter appears to have a significant influence on the electron density at the heme site, as suggested by EPR, even resulting in an altered interaction between the iron and the fifth ligand at the proximal side. These differences seem to be due to a single-point mutation, which is the only structural aspect evidently differentiating the two isoforms. More interestingly, the oxygen level appeared to be able to modulate these intrinsic dynamical differences, larger with decreasing pO_2 .

However, we want to stress that the same mutation in a Mb, other than the human's, is not necessarily expected to lead to the same differences. Its effectiveness should be ultimately dependent upon the subtle interplay between the biophysical modifications induced by the mutation and the intrinsic dynamics of the protein under investigation, thus being possibly strongly sequence specific.

How these differences are ultimately translated into an alternative or complementary role for the two more expressed human Mb isoforms in severe hypoxia still needs to be elucidated, but the road to take is extremely interesting and calls for further investigations.

■ ASSOCIATED CONTENT

Supporting Information

Figures S1–S7, movie S1, and additional details about the computational methods. This material is available free of charge via the Internet at <http://pubs.acs.org>.

■ AUTHOR INFORMATION

Corresponding Author

matteo.ceccarelli@dsf.unica.it; maristella.gussoni@unimi.it

Present Address

✉E.S.: École Polytechnique Fédérale de Lausanne (EPFL-IBI), Switzerland

Notes

The authors declare no competing financial interest.

■ ACKNOWLEDGMENTS

We thank the CINECA supercomputer center for CPU time allocation to this project (ISCRA-B-HP10BRSNYP). We gratefully acknowledge the funding from National Research Project (PRIN 2006–2008 prot. 2006059902) of the Italian Ministry for the University (MIUR) that allowed us to start working on this subject.

■ REFERENCES

- (1) Brunori, M.; Bourgeois, D.; Vallone, B. *J. Struct. Biol.* **2004**, *147*, 223–234.
- (2) Frauenfelder, H.; McMahon, B. H.; Fenimore, P. W. *Proc. Natl. Acad. Sci. U.S.A.* **2003**, *100*, 8615–8617.
- (3) Kooymann, G. L.; Pongonis, P. *J. Annu. Rev. Physiol.* **1998**, *60*, 19–32.
- (4) Springer, B.; Sligar, S.; Olson, J.; Phillips, G. *Chem. Rev.* **1994**, *94*, 699–714.
- (5) Wittenberg, B. A.; Wittenberg, J. B. *Annu. Rev. Physiol.* **1989**, *51*, 857–878.
- (6) UniProt: *Universal Protein Resource*. <http://www.uniprot.org/> (accessed September 2012).
- (7) Cossins, A. R.; Williams, D. R.; Foulkes, N. S.; Berenbrink, M.; Kipar, A. *J. Exp. Biol.* **2009**, *212*, 627–638.
- (8) Gelfi, C.; De Palma, S.; Ripamonti, M.; Wait, R.; Eberini, I.; Bajracharya, A.; Marconi, C.; Schneider, A.; Hoppeler, H.; Cerretelli, P. *FASEB J.* **2004**, *18*, 612–614.
- (9) Moore, L. G.; Zamudio, S.; Zhuang, J.; Droma, T.; Shohet, R. V. *High Alt. Med. Biol.* **2002**, *3*, 39–47.
- (10) Kristiansen, G.; Hu, J.; Wichmann, D.; Stiehl, D. P.; Rose, M.; Gerhardt, J.; Bohnert, A.; Ten Haaf, A.; Moch, H.; Raleigh, J.; et al. *J. Biol. Chem.* **2011**, *286*, 43417–43428.
- (11) Flonta, S. E.; Arena, S.; Pisacane, A.; Michieli, P.; Bardelli, A. *Am. J. Pathol.* **2009**, *175*, 201–206.
- (12) Brunori, M. *Trends Biochem. Sci.* **2001**, *26*, 21–23.
- (13) Shiva, S.; Huang, Z.; Grubina, R.; Sun, J.; Ringwood, L. A.; MacArthur, P. H.; Xu, X.; Murphy, E.; Darley-Usmar, V. M.; Gladwin, M. T. *Circ. Res.* **2007**, *100*, 654–661.
- (14) Liu, Q.; Gross, S. S. *Methods Enzymol.* **1996**, *268*, 311–324.
- (15) Knowles, R. G.; Moncada, S. *Biochem. J.* **1994**, *298*, 249–258.
- (16) Shiva, S. *Nitric oxide* **2010**, *22*, 64–74.
- (17) Totzeck, M.; Hendgen-Cotta, U. B.; Rammos, C.; Petrescu, A. M.; Meyer, C.; Balzer, J.; Kelm, M.; Rassaf, T. *Nitric oxide* **2012**, *26*, 211–216.
- (18) Cossins, A.; Berenbrink, M. *Nature* **2008**, *454*, 416–417.
- (19) Hendgen-Cotta, U. B.; Flögel, U.; Kelm, M.; Rassaf, T. *J. Exp. Biol.* **2010**, *213*, 2734–2740.
- (20) Chen, Q.; Moghaddas, S.; Hoppel, C. L.; Lesnefsky, E. J. *J. Pharmacol. Exp. Therap.* **2006**, *319*, 1405–1412.
- (21) Rassaf, T.; Flögel, U.; Drexhage, C.; Hendgen-Cotta, U.; Kelm, M.; Schrader, J. *Circ. Res.* **2007**, *100*, 1749–1754.
- (22) Huang, Z.; Shiva, S.; Kim-shapiro, D. B.; Patel, R. P.; Ringwood, L. A.; Irby, C. E.; Huang, K. T.; Ho, C.; Hogg, N.; Schechter, A. N.; Gladwin, M. T. *J. Clinical Inv.* **2005**, *115*, 2099–2107.
- (23) Cosby, K.; Partovi, K. S.; Crawford, J. H.; Patel, R. P.; Reiter, C. D.; Martyr, S.; Yang, B. K.; Waclawiw, M. A.; Zalos, G.; Xu, X.; et al. *Nat. Med.* **2003**, *9*, 1498–1505.
- (24) Rossi-Fanelli, A.; Antonini, E. *Arch. Biochem. Biophys.* **1958**, *77*, 478–492.
- (25) Rossi-Fanelli, A.; Antonini, E. *Arch. Biochem. Biophys.* **1956**, *66*, 587–590.

- (26) *GeneCards—The Human Gene Compendium*. www.genecards.org (accessed September 2012).
- (27) Boulton, F. E.; Huntsman, R. G.; Lorkin, P. A.; Lehmann, H. *Nature* **1969**, *223*, 832–833.
- (28) Boulton, F. E.; Huntsman, R. G.; Romero Herrera, A. E.; Lorkin, P. A.; Lehmann, H. *Biochim. Biophys. Acta* **1971**, *229*, 871–876.
- (29) Boulton, F. E.; Huntsman, R. G.; Yawson, G. I.; Romero Herrera, A. E.; Lorkin, P. A.; Lehmann, H. *Br. J. Haematol.* **1971**, *20*, 69–74.
- (30) Boulton, F. E.; Huntsman, R. G.; Romero Herrera, A. E.; Lorkin, P. A.; Lehmann, H. *Biochim. Biophys. Acta* **1971**, *229*, 716–719.
- (31) Reynafarje, B. *J. Appl. Physiol.* **1962**, *17*, 301–305.
- (32) Beall, C. M. *Proc. Natl. Acad. Sci. U.S.A.* **2007**, *104*, 8655–8660.
- (33) Marconi, C.; Marzorati, M.; Sciuto, D.; Ferri, A.; Cerretelli, P. *J. Physiol.* **2005**, *569*, 667–675.
- (34) Bourgeois, D.; Vallone, B.; Arcovito, A.; Sciarra, G.; Schotte, F.; Anfinrud, P. A.; Brunori, M. *Proc. Natl. Acad. Sci. U.S.A.* **2006**, *103*, 4924–4929.
- (35) Bourgeois, D.; Vallone, B.; Schotte, F.; Arcovito, A.; Miele, A. E.; Sciarra, G.; Wulff, M.; Anfinrud, P.; Brunori, M. *Proc. Natl. Acad. Sci. U.S.A.* **2003**, *100*, 8704–8709.
- (36) Elber, R. *Curr. Op. Struct. Biol.* **2010**, *20*, 162–167.
- (37) Blouin, G. C.; Schweers, R. L.; Olson, J. S. *Biochemistry* **2010**, *49*, 4987–4997.
- (38) Ceccarelli, M.; Anedda, R.; Casu, M.; Ruggerone, P. *Proteins* **2008**, *71*, 1231–1236.
- (39) Olson, J. S.; Soman, J.; Phillips, G. N. *IUBMB Life* **2007**, *59*, 552–562.
- (40) Cohen, J.; Schulten, K. *Biophys. J.* **2007**, *93*, 3591–3600.
- (41) Agmon, N. *Biophys. J.* **2004**, *87*, 1537–1543.
- (42) Scott, E. E.; Gibson, Q. H.; Olson, J. S. *J. Biol. Chem.* **2001**, *276*, 5177–5188.
- (43) Perutz, M. F.; Matthews, F. S. *J. Mol. Biol.* **1966**, *21*, 199–202.
- (44) Scorciapino, M. A.; Wallon, C.; Ceccarelli, M. *Theor. Chem. Acc.* **2011**, *130*, 1105–1114.
- (45) Hoy, J. a.; Robinson, H.; Trent, J. T.; Kakar, S.; Smagghe, B. J.; Hargrove, M. S. *J. Mol. Biol.* **2007**, *371*, 168–179.
- (46) Dasmeh, P.; Kepp, K. P. *Comp. Biochem. Physiol., Part A: Mol. Integr. Physiol.* **2012**, *161*, 9–17.
- (47) Gussoni, M.; Scorciapino, M. A.; Vezzoli, A.; Anedda, R.; Greco, F.; Ceccarelli, M.; Casu, M. *Biochim. Biophys. Acta* **2011**, *1814*, 1919–1929.
- (48) Scorciapino, M. A.; Robertazzi, A.; Casu, M.; Ruggerone, P.; Ceccarelli, M. *J. Am. Chem. Soc.* **2009**, *131*, 11825–11832.
- (49) Scorciapino, M. A.; Robertazzi, A.; Casu, M.; Ruggerone, P.; Ceccarelli, M. *J. Am. Chem. Soc.* **2010**, *132*, 5156–5163.
- (50) Yonetani, T.; Yamamoto, H.; Erman, J. E.; Leigh, J. S. J.; Reed, G. H. *J. Biol. Chem.* **1972**, *247*, 2447–2455.
- (51) Kon, H. *J. Biol. Chem.* **1968**, *243*, 4350–4357.
- (52) Ingram, D. J.; Kendrew, J. C. *Nature* **1956**, *178*, 905–906.
- (53) Hubbard, S. R.; Hendrickson, W. A.; Lambright, D. G.; Boxer, S. G. *J. Mol. Biol.* **1990**, *213*, 215–218.
- (54) Lindorff-Larsen, K.; Piana, S.; Palmo, K.; Maragakis, P.; Klepeis, J. L.; Dror, R. O.; Shaw, D. E. *Proteins* **2010**, *78*, 1950–1958.
- (55) Jorgensen, W.; Chandrasekhar, J.; Madura, J.; Impey, R.; Klein, M. *J. Chem. Phys.* **1983**, *79*, 926–936.
- (56) Harvey, M.; Giupponi, G.; De Fabritiis, G. *J. Chem. Theory Comput.* **2009**, *5*, 1632–1639.
- (57) Mezei, M. *J. Comput. Chem.* **2010**, *31*, 2658–2668.
- (58) Kleywegt, G. J.; Zou, J. Y.; Kjeldgaard, M.; Jones, T. A. In *International Tables for Crystallography Vol.F*; Arnold, E., Himmel, D. M., Rossmann, M. G., Eds.; Kluwer Academic Publishers: Dordrecht, The Netherlands, 2001; pp 353–356 and 366–367.
- (59) Kleywegt, G. J.; Jones, T. A. *Acta Crystallogr., Sect. D: Biol. Crystallogr.* **1994**, *50*, 178–185.
- (60) Impey, R. W.; Madden, P. a.; McDonald, I. R. *J. Phys. Chem.* **1983**, *87*, 5071–5083.
- (61) Marchi, M.; Sterpone, F.; Ceccarelli, M. *J. Am. Chem. Soc.* **2002**, *124*, 6787–6791.
- (62) Tiravanti, E.; Samouilov, A.; Zweier, J. L. *J. Biol. Chem.* **2004**, *279*, 11065–11073.
- (63) Dikalov, S.; Fink, B. *Methods Enzymol.* **2005**, *396*, 597–610.
- (64) Nutt, D. R.; Smith, J. C. *J. Am. Chem. Soc.* **2008**, *130*, 13066–13073.
- (65) Zhang, L.; Wang, L.; Kao, Y. T.; Qiu, W.; Yang, Y.; Okobiah, O.; Zhong, D. *Proc. Natl. Acad. Sci. U.S.A.* **2007**, *104*, 18461–18466.
- (66) Fenimore, P. W.; Frauenfelder, H.; McMahon, B. H.; Parak, F. G. *Proc. Natl. Acad. Sci. U.S.A.* **2002**, *99*, 16047–16051.
- (67) Sterpone, F.; Stirnemann, G.; Hynes, J. T.; Laage, D. *J. Phys. Chem. B* **2010**, *114*, 2083–2089.
- (68) Frauenfelder, H.; Chen, G.; Berendzen, J.; Fenimore, P. W.; Jansson, H.; McMahon, B. H.; Strope, I. R.; Swenson, J.; Young, R. D. *Proc. Natl. Acad. Sci. U.S.A.* **2009**, *106*, 5129–5134.
- (69) Witting, P. K.; Douglas, D. J.; Mauk, A. G. *J. Biol. Chem.* **2001**, *276*, 3991–3998.
- (70) Ballhausen, C. J. In *Introduction to ligand field theory*; Mc Graw-Hill: New York, 1962.
- (71) Kon, H.; Kataoba, N. *Biochemistry* **1969**, *8*, 4757–4761.
- (72) Morse, R. H.; Chan, S. I. *J. Biol. Chem.* **1980**, *255*, 7876–7882.
- (73) Ascenzi, P.; Giacometti, G. M.; Antonini, E.; Rotilio, G.; Brunori, M. *J. Biol. Chem.* **1981**, *256*, 5383–5386.
- (74) Van Faassen, E. E.; Bahrami, S.; Feelisch, M.; Hogg, N.; Kelm, M.; Kim-shapiro, D. B.; Kozlov, A. V.; Li, H.; Lundberg, J. O.; Mason, R.; et al. *Med. Res. Rev.* **2009**, *29*, 683–741.
- (75) Sharma, V. S.; Isaacson, R. A.; John, M. E.; Waterman, M. R.; Chevion, M. *Biochemistry* **1983**, *22*, 3897–3902.
- (76) Kobayashi, K.; Tamura, M.; Hayashi, K. *Biochemistry* **1982**, *21*, 729–732.
- (77) Gow, A. J.; Luchsinger, B. P.; Pawloski, J. R.; Singel, D. J.; Stamler, J. S. *Proc. Natl. Acad. Sci. U.S.A.* **1999**, *96*, 9027–9032.
- (78) Ford, P. C. *Pure Appl. Chem.* **2004**, *76*, 335–350.